THE MODELING OF UNSTEADY TURBULENT FLOWS IN TURBOMACHINES

FRANCO MAGAGNATO

Department of Fluid Flow Machinery,
University of Karlsruhe,
Kaiserstrasse 12, D-76128 Karlsruhe, Germany
magagnato@mach.uni-karlsruhe.de

Abstract: The suitability of existing models for the simulation of flow through turbomachines is investigated and compared with a recently proposed adaptive turbulence model. Discussed are the improvements in accuracy that can be achieved by using non-linear turbulence models and unsteady calculations. The adaptive turbulence model is based on two equation turbulence modeling. It uses the temporal and spatial scales of the flow field to automatically adapt itself to the unresolved turbulent fluctuations. At its asymptotic limits it reduces either to a Direct Numerical Simulation – when the turbulent scales are in the order of the Kolmogorov micro scale – or to a standard two equation model – when the fluctuations are not resolved at all.

In order to compare the quality of the presented models two cases have been considered: the flow past a cylinder and a subsonic as well as transonic flow past the VKI turbine blade. Calculations have been performed for each case using all the models and the results have been compared with measurements. The unsteady calculations gave better agreement with the experimental data demonstrating the superiority over steady state calculations for turbomachines.

Keywords: turbulence, compresible, unsteady, RANS, LES

1. Introduction

The simulation of complex flow fields, especially in turbomachines, implies a compromise between the attained accuracy and required computational resources. From this point of view ignoring the time evolution was for a while an acceptable approximation. The comparison of the results obtained in the past with the experimental work showed that for this special case the approximation was too coarse. The results of steady state calculations can not predict the pressure loss accurately enough. The question was if an unsteady approach is more suitable. It has recently been shown that the unsteady approach gave an improved agreement of the calculated flow field with the measurement data compared to steady state computations (Chen and Leschziner [1], Magagnato [2]). The prediction of the large scale vortices generated by thick trailing edges of turbine blades plays an important role here.

In another work attention was drawn toward developing a model that would permit the calculation of an unsteady simulation of flows in turbomachines with acceptable computational effort (time and memory usage; Magagnato and Gabi [3]).

2. Turbulence models

The key point for such a strongly three dimensional and unsteady flow is turbulence modeling. For the Reynolds number of practical interest, this flow is characterised by a wide range of length and time scales. Resolving all scales by a time accurate and three-dimensional calculation with very high temporal and spatial resolution (DNS) seems to be impossible in the near future (Piomelli [4]). On the other hand, the statistical approach is based on the decomposition into mean values (averaged over time, space, phase or ensemble) and fluctuations. Insertion of this decomposition into the Navier-Stokes equations leads to the Reynolds-averaged Navier-Stokes (RANS) equations that contain, beside the averaged terms, also terms like the Reynolds stresses that cannot be represented uniquely in terms of the mean quantities. The system is no longer closed and the required closure is attained only through introduction of approximations that prescribes the Reynolds stresses in terms of the mean values. For steady state calculations (suitable only for statistical steady flow) the closed systems is solved.

One can also resolve a fraction of the fluctuations by an unsteady RANS (URANS) calculation. The common practice is to use the same turbulence models as for steady state calculations. This is an acceptable approach as long as only a small fraction of the fluctuation is resolved ($< 10\%$). But calculations resolving a larger part of the turbulent fluctuations require a different model, which pays attention to the amount of fluctuations resolved. This is certainly true for three-dimensional calculations. For two-dimensional unsteady calculations the situation is less clear. While a two-dimensional calculation resolves also some fluctuations it is generally accepted that turbulence is always three-dimensional in nature.

Large Eddy Simulation (LES) is a widely accepted and promising numerical approach. It is time dependent and three dimensional and requires fine grids but coarser than those for DNS because not all time and space scales are resolved. With the aid of spatial and temporal filters applied in the inertial subrange of the turbulent energy spectrum, the flow is decomposed spatially into a part that is resolved and a part that must be modeled (sub-grid scale model SGS).

An algebraic SGS model (Smagorinsky [5]) and variants of it [6] are very often used. It has demonstrated good predictive capabilities for fairly complex flow fields when used in conjunction with a relatively high resolution of the flow field or at relatively low Reynolds numbers. A disadvantage of it is that one must adapt the proportionality constant individually for different flow fields. A better strategy is the dynamic SGS model of Germano *et al.* [7]. It extrapolates this constant with the help of the resolved flow field.

All SGS models known by the author can only be applied inside the inertial subrange. In the limit of steady state simulations they model the turbulence completely wrong (Turbulent stresses $\rightarrow \infty$).

For a less demanding URANS calculation a model is required, which can handle a smaller fraction of the turbulence spectrum on a coarser grid.

In [1] and [2] calculations of the flow field in turbomachines with linear two-equation eddy viscosity models (Launder and Sharma [8] Speziale [9]) have been made. Since the agreement with the measurements were poor, effort was concentrated on the development and application of non-linear models. The idea was to make a compromise between the robustness of linear models and the potentially greater accuracy of Reynolds stress models

without a smaller computational effort compared to the previous one. This was achieved through the introduction of a non-linear term in the stress strain relation on the right side in equation:

$$-\rho\overline{u_i u_j} = -\frac{2}{3}\rho k\delta_{ij} + \mu_t S_{ij} + F_{ij}(S_{ij}^2, S_{ij}^3, \ldots), \tag{1}$$

S_{ij} denotes the strain tensor.

Speziale [10] proposed a model that uses only quadratic terms in the formulation of the stress/strain relation (for details see Magagnato [11]). Consequently, the improvements in accuracy were small [12]. The inclusion of the Oldroyd derivative was found [11] to be a numerical weak point due to stability problems and higher computational effort. A turbulence model using also cubic terms was proposed by Craft, Launder and Suga [13]. Its numerical stability is as good as that of linear two-equation models. The price for the augmented accuracy is also low (5–10% cpu-time overhead with respect to the linear models compared to 30–40% reclaimed by the model of Speziale). As the best candidate (with respect to stability, economy, usefulness and portability), it has been chosen by the author of this paper as starting point of further developments.

One improvement in [3] was the transformation of the k-ε into an equivalent k-τ formulation. The τ-equation is numericaly robust because inside the boundary layer τ has an almost linear distribution. The corresponding wall boundary condition $\tau = 0$ helps also to improve the robustness of the calculation.

In order to make the numerical scheme suitable for simulating unsteady compressible flows a great deal of attention must be paid to the implementation of non-reflecting boundary conditions [14]. From the variety of BC proposed in the literature we have chosen the relatively simple one from Rudy and Strikwerda [15] and the much more sophisticated one of Poinsot and Lele [16] to implement and to test. Both showed an effective suppression of the pressure reflection at the downstream as well as upstream boundaries when applied to simple and academic flow fields.

When applied to the subsonic flow field of the Genoa test case [17], the BC of Poinsot and Lele showed only small differences of the calculated solution compared to that calculated with the conventional BC of constant static pressure. The reason for this was due to the relatively far distant location of the boundary condition relative to the vortical flow around the turbine blade. The extra computational time required for the non-reflecting BC is in the order of 30–50% for the dual time stepping method in comparison with the conventional BC.

In order to model only the unresolved fraction of the turbulent fluctuations, Speziale [18] has proposed an approch that is based on the fact that the differences that exist between the traditional Reynolds averaging and the spatial filter in LES disappear in the limit of high cell Reynolds number.

Spalart *et al.* [19] proposed a method called DES (Detached Eddy Simulation) for the simulation of a high Reynolds number flow around an airfoil as an alternative to a conventional LES computation that proved to be too expensive in this case. DES applies URANS in the boundary layer and LES in the region of massive separation. For making that possible in a single formulation he replaced the length scale in the Spalart and Allmaras one equation model [20] with the minimum between the local distance from the wall and the grid spacing. In this way the model adapts automatically one or the other form according to the spatial position and resolution.

The adaptive model proposed by Magagnato and Gabi [3] uses the two equation non-linear model of Craft, Launder and Suga [13] that has proved its advantages in URANS simulations [1], [2]. In addition a stochastic backscatter model based on the unresolved turbulent kinetic energy was included. The adaptive character is manifested through:

– asymptotical convergence toward a statistical model in the limit of high cell Reynolds numbers,
– approach to a direct numerical simulation when the cell Reynolds number reaches the Kolmogorov length scale.

The main idea is to split the turbulent dissipation rate ε (or the time scale τ) like the turbulent kinetic energy into two parts (Equations (2) and (3)). In an unsteady calculation the fraction of the turbulent kinetic energy spectrum larger than the numerical resolution is resolved and the unresolved part must be modeled. Accordingly, also ε (or the time scale τ) will be split into a resolved and an unresolved part:

$$k = k' + \bar{k} \tag{2}$$

$$\varepsilon = \varepsilon' + \ddot{\varepsilon} \tag{3}$$

The resolved dissipation rate and the respective resolved turbulent time scale are modeled via the relation valid for isotropic, turbulent high Reynolds number flows:

$$\bar{\varepsilon} = \frac{k'^{3/2}}{L_\Delta} \tag{4}$$

According to this the mean dissipation rate of the turbulent kinetic energy is proportional to the unresolved turbulent kinetic energy k' divided by the turbulent length scale L_Δ. Consequently, the resolved turbulent time scale becomes:

$$\bar{\tau} = \frac{L_\Delta}{\sqrt{k'}} \tag{5}$$

The unresolved turbulent kinetic energy and turbulent dissipation rate (respectively turbulent time scale) will be calculated by transport equations.

For the approximation of the turbulent length scale, one must assure that the temporal filter as well as the spatial filter is less or equal to the temporal or spatial resolution. Therefore the filter will be in this case the maximum between the spatial (L_s) and the temporal (L_t) filter width:

$$L_\Delta = \max \left\{ \begin{array}{l} L_s \\ L_t \end{array} \right\} \tag{6}$$

The spatial length scale will be approximated like in conventional LES. Here the grid spacing is chosen as an appropriate spatial length scale so that L_s will be calculated from the cell sizes in the coordinate direction Δx, Δy, Δz with equation:

$$L_s = 2 \cdot \sqrt[3]{\Delta x \cdot \Delta y \cdot \Delta z} \tag{7}$$

The temporal filter is adapted to the local conditions through $|u|$ the velocity in the node and will be calculated according to the equation:

$$L_t = |u| \cdot \Delta t \tag{8}$$

where Δt is the time step.

We must accentuate that this splitting is not specific to the turbulence model chosen in our approach. Because this splitting can be introduced in any turbulence model that contains a transport equation for k and ε (τ or ω, respectively), the way to improve the adaptive model through better models of this type is open.

The following model results from mathematical transformation of the model in [13] into a k-τ turbulence model:

$$\frac{\partial(\rho k')}{\partial t} + \frac{\partial(\rho u_i k')}{\partial x_i} = \frac{\partial}{\partial x_i}\left((\mu+\mu_k)\frac{\partial k'}{\partial x_i}\right) + P_k - \rho\frac{k'\left(1+\frac{\tau'\sqrt{k'}}{L_\Delta}\right)}{\tau'},$$

$$\frac{\partial(\rho\tau')}{\partial t} + \frac{\partial(\rho u_i\tau')}{\partial x_i} = \frac{\partial}{\partial x_i}\left((\mu+\mu_\tau)\frac{\partial\tau'}{\partial x_i}\right) + (1-c_{\varepsilon 1})\cdot\frac{\tau'}{k'}P_k + \rho\left(c_{\varepsilon 2}-\left(1+\frac{\tau'\sqrt{k'}}{L_\Delta}\right)\right)$$

$$+ \frac{2}{k'}(\mu+\mu_\tau)\frac{\partial k'}{\partial x_i}\frac{\partial\tau'}{\partial x_i} - \frac{2}{\tau'}(\mu+\mu_\tau)\frac{\partial\tau'}{\partial x_i}\frac{\partial\tau'}{\partial x_i} - 0.06\cdot S\cdot\tau'^3\left(\frac{\partial^2 u_i}{\partial x_k\partial x_j}\right)^2,$$

$$\mu_t = \rho\cdot c_\mu\cdot f_\mu\cdot k'\cdot\tau', \qquad c_\mu = \frac{0.3}{1+0.35\cdot S^{3/2}}\left(1-\exp\left(-\frac{0.36}{\exp(-0.75\cdot S)}\right)\right), \qquad (9)$$

$$P_k = -\rho\overline{u_i'u_j'}\frac{\partial u_i}{\partial x_j}, \qquad S = \tau'\sqrt{S_{ij}S_{ij}/2}, \qquad S_{ij} = \frac{\partial u_i}{\partial x_j} + \frac{\partial u_j}{\partial x_i} - \frac{2}{3}\frac{\partial u_i}{\partial x_i}\delta_{ij},$$

$$\Omega_{ij} = \frac{\partial u_i}{\partial x_j} - \frac{\partial u_j}{\partial x_i}, \qquad f_\mu = 1-\exp\left(-\left(\frac{\mathrm{Re}_t}{90}\right)^{1/2}-\left(\frac{\mathrm{Re}_t}{400}\right)^2\right),$$

$$-\rho\overline{u_i'u_j'} = \mu_t\cdot S_{ij} - \frac{2}{3}k'\delta_{ij} - c_1\mu_t\tau'(S_{ik}S_{kj} - \frac{1}{3}S_{kl}S_{kl}\delta_{ij}) - c_2\mu_t\tau'(\Omega_{ik}S_{kj}+\Omega_{jk}S_{kj})$$

$$-c_3\mu_t\tau'\left(\Omega_{ik}\Omega_{jk} - \frac{1}{3}\Omega_{kl}\Omega_{kl}\delta_{ij}\right) + c_\mu\mu_t\tau'^2\left\{c_4\left[S_{ki}\Omega_{lj}+S_{kj}\Omega_{li}-\frac{2}{3}S_{km}\Omega_{lm}\delta_{ij}\right]S_{kl}\right.$$

$$\left. +c_5\left[S_{ik}S_{jl}-\frac{1}{3}S_{mk}S_{ml}\delta_{ij}\right]S_{kl} + c_6 S_{ij}S_{kl}S_{kl} + c_7 S_{ij}\Omega_{kl}\Omega_{kl}\right\}$$

with the following constants:

c_μ	c_1	c_2	c_3	c_4	c_5	c_6	c_7
0.09	−0.1	0.1	0.26	−0.081	0	0.0405	−0.0405

Appropriate boundary conditions for the unresolved turbulent kinetic energy and turbulent time scale of this model must now be constructed. Following the same idea they must reduce to the standard boundary condition used for RANS or to the specification of fluctuations in the limit of a DNS.

The following approximation will be used to accomplish this.

The resolved part of the turbulent kinetic energy is applied in the simulation as disturbances of the freestream velocity field with a random white noise, while the unresolved part is used as the boundary condition of the transport equation of k'. The wave number of the grid scale determines the split point $\kappa_\Delta = \pi/L_\Delta$. Because the splitting is done with the assumption that in the freestream the energy spectrum of the turbulent kinetic energy is conforming to the Kolmogorov −5/3 power law, κ_Δ will by varying between the wavenumber
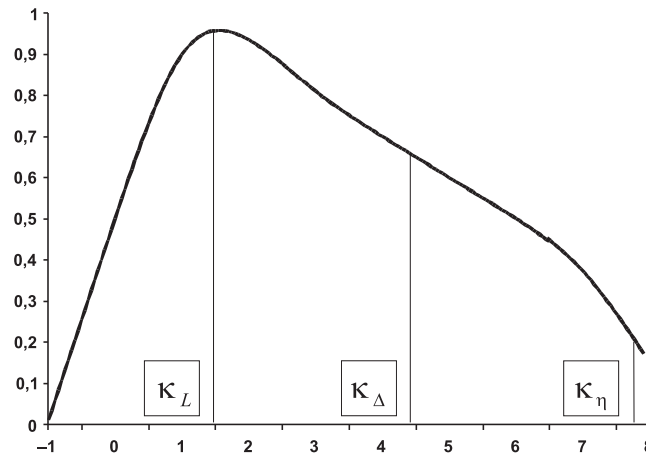
Figure 1. Spectrum of turbulent energy

of Kolmogorov scale $\kappa_\eta = \pi/L_\eta$ and that of the characteristic scale $\kappa_L = \pi/L$ built with the length scale usually used in a conventional two equation model (see Figure 1).

Approximating the Kolomogorov wave number by equation:

$$\kappa_\eta = \kappa_L \left(\frac{\rho_\infty L_T \sqrt{k_\infty}}{\mu_\infty} \right)^{-3/4} \tag{10}$$

and noting that the splitting will be done by integrating the spectrum between κ_L and κ_η with a linear weighting of the split point κ_Δ the boundary condition for k' becomes:

$$k' = k_\infty \frac{\kappa_\eta^{-2/3} - \kappa_\Delta^{-2/3}}{\kappa_\eta^{-2/3} - \kappa_L^{-2/3}} \tag{11}$$

The boundary condition for τ' is:

$$\tau' = \frac{L_\Delta}{\sqrt{k_\infty}} \tag{12}$$

It's evident that for $\kappa_\Delta = \kappa_L \rightarrow k' = k_\infty$ results and for $\kappa_\Delta = \kappa_\eta \rightarrow k' = 0$ so that the limits are recovered.

The inclusion of a backscatter model is an important feature of the proposed model. In spite of the fact that the bi-directional character of the energy exchange between the large scale and small scale motion is well known only the transfer from the large scale to the small one called forward scatter is usually modeled (Lilly [21]). Among a few models that account for the reverse transfer called backscatter (Leith [22], Mason and Thomas [23]), Schumann [24] proposed a model which gives good results for decaying isotropic turbulence. From that model we derived a backscatter model based on the unresolved turbulent kinetic energy k' and the unresolved turbulent time scale τ'. This model also has the correct asymptotical behavior so that in the limit of a DNS the velocity disturbances disappear and in the limit of a RANS they disappear as well. In between it should have a monotonic behavior with a maximum in the inertial range.

The backscatter model reads:

$$-(\rho \overline{u'_i u'_j})_B = -\rho v'_i v'_j + \frac{2}{3} \rho k' \delta_{ij} \tag{13}$$

The stochastic character of the backscatter – in contrast to the dissipative character of the forward scatter modeled by an eddy viscosity model – is modeled through the random

velocities v_i that are calculated at each time step using the values of the unresolved turbulent kinetic energy and turbulent time scale in a Langevin type equation:

$$(v'_i)^n = (v'_i)^{n-1} \left(1 - \frac{\Delta t}{\tau'} \right) + \left(\frac{\Delta t}{\tau'} \left(2 - \frac{\Delta t}{\tau'} \right) \frac{2}{3} k' \right)^{1/2} Z_i^n \tag{14}$$

Z_i here is an independent random number in the range $(-1, 1)$.

With the initialisation at first step

$$(v'_i)^0 = \left(\frac{2}{3} k' \right)^{1/2} \tag{15}$$

the random disturbance becomes:

$$\left\langle \left((v'_i)^n \right)^2 \right\rangle = \frac{2}{3} k' \tag{16}$$

Δt is the time step of the numerical scheme and τ' is defined in Equation (12). It is obvious that for $k' = 0$ in the limit of DNS $v_i = 0$. When $L_\Delta = \infty$ then $t' = \infty$ and $(v'_i)^n = (v'_i)^0$ for all time steps and the stochastic stresses of the backscatter model are zero. The relation for the calculation of the complete Reynolds stresses (or subgrid-scale stresses) for the k-τ model then reads:

$$-\rho \overline{u'_i u'_j} = \rho c_\mu k' \tau' S_{ij} - \frac{2}{3} \rho k' \delta_{ij} - \rho v'_i v'_j + \frac{2}{3} \rho k' \delta_{ij} \tag{17}$$

and for the k-ε model:

$$-\rho \overline{u'_i u'_j} = \rho c_\mu \frac{k'^2}{\varepsilon'} S_{ij} - \frac{2}{3} \rho k' \delta_{ij} - \rho v'_i v'_j + \frac{2}{3} \rho k' \delta_{ij} \tag{18}$$

3. Numerical method

A block structured finite volume and cell centered scheme has been used for all calculations [25].

For the URANS calculation a dual time stepping scheme proposed by Jameson [26] and modified by Arnone *et al.* [27] has been used. In this very efficient and paralellised scheme, the time discretisation is made implicit so that the time step is determined by physical considerations only and not by numerical ones. Stability restrictions are removed so that acceleration techniques can be applied instead of traditional time consuming factorisation (*i.e.* alternate direction implicit and lower/upper schemes). In order to achieve this the governing equation must be reformulated so that it can be treated as a modified steady state problem in a fictitious time τ.

For the calculation that uses the adaptive model a 4th order Runge Kutta scheme for integration in time, and a 4th order cell centered scheme for the spatial integration has been adopted [28]. In this case the computational time for the new model is negligible compared to a conventional two equation model, provided that the filter length L_s is calculated only once at the initialisation and stored into a permanent array.

The convergence acceleration methods used are the full multigrid method [29], an implicit residual averaging technique and local time stepping (see Magagnato [25]). All methods are implemented into our own CFD code called SPARC using MPI for paralellisation of the calculation. The calculations have been made mostly on an IBM SP2 using 64 processors in parallel with an efficiency of 93%.

4. Calculations

The proposed turbulence model has been investigated on two flow fields for which accurate measurement are available in order to evaluate the accuracy and to compare with the standard turbulence models. The first one is the flow field around a cylinder for which the experimental measurements have been conducted by Lienhard [30] and Cantwell and Coles [31]. Steady state simulations of this case have been done by many researchers in the past showing poor agreement with the experiment.

The freestream velocity for this flow was $u = 21.2$ m/s and together with diameter of the cylinder a Reynolds number of $\mathrm{Re}_D = 140\,000$ results. The turbulence level Tu was 0.6%. Two two-dimensional URANS simulations, one with a linear model (Launder and Sharma [8]) and one with the non-linear model proposed by Craft, Launder and Suga [13] and one LES using the adaptive turbulence model have been conducted.

The generated grid for this flow field was of OC-type (see Figure 2).
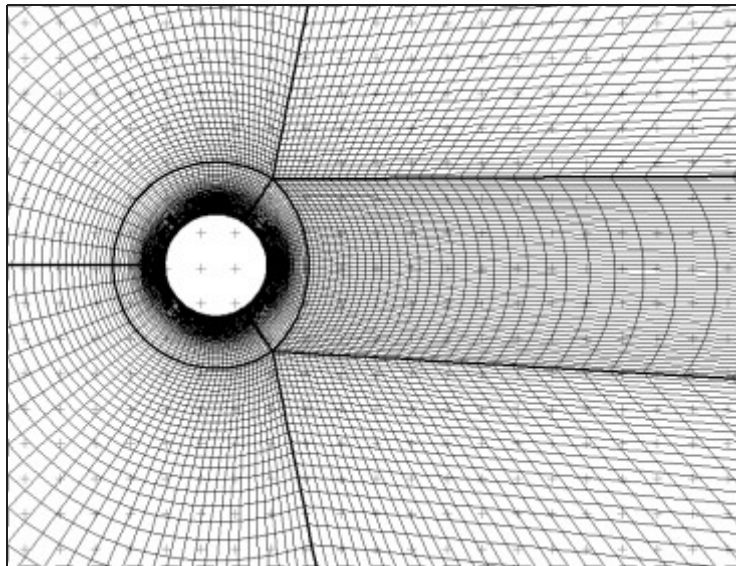
Figure 2. Computational grid for circular cylinder

For the URANS simulations the two-dimensional variant of SPARC has been used with a total of 52 000 points in the finest grid. Mesh independence has been demonstrated by performing calculation with approximately 13 000 points that showed almost the same values ($< 2\%$) as in the finest grid.

For the LES calculation with the adaptive model a three dimensional extension of the grid has been used. In the spanwise direction the cylinder has been extended three diameters in order to resolve the crossflow correlation sufficiently. With approximately 18 000 points in the symmetry plane and 97 in the spanwise direction the grid consists of about 1 700 000 points.

The unknown turbulence length scale in the free stream was approximated so that the resulting eddy viscosity was in the order of the molecular viscosity. The turbulence level was then used for the specification of the total turbulent kinetic energy and the turbulent

length scale in the freestream for the statistical models. For LES with the adaptive model the above mentioned boundary conditions have been used.

Because of the inability of all eddy viscosity models to predict natural transition, transition must be prescribed explicitly. The transition point has been fixed at $\alpha = 80°$.

The unsteady two-dimensional calculation on the coarse grid (4 500 points) showed no vortex shedding due to the high numerical damping of the fluctuations. In the semi-refined grid the vortices are generated in the wake but dissipate after about four diameters downstream of the cylinder (Figure 3).

Level	U
21	80.0
20	74.5
19	69.0
18	63.5
17	58.0
16	52.5
15	47.0
14	41.5
13	36.0
12	30.5
11	25.0
10	19.5
9	14.0
8	8.5
7	3.0
6	-2.5
5	-8.0
4	-13.5
3	-19.0
2	-24.5
1	-30.0
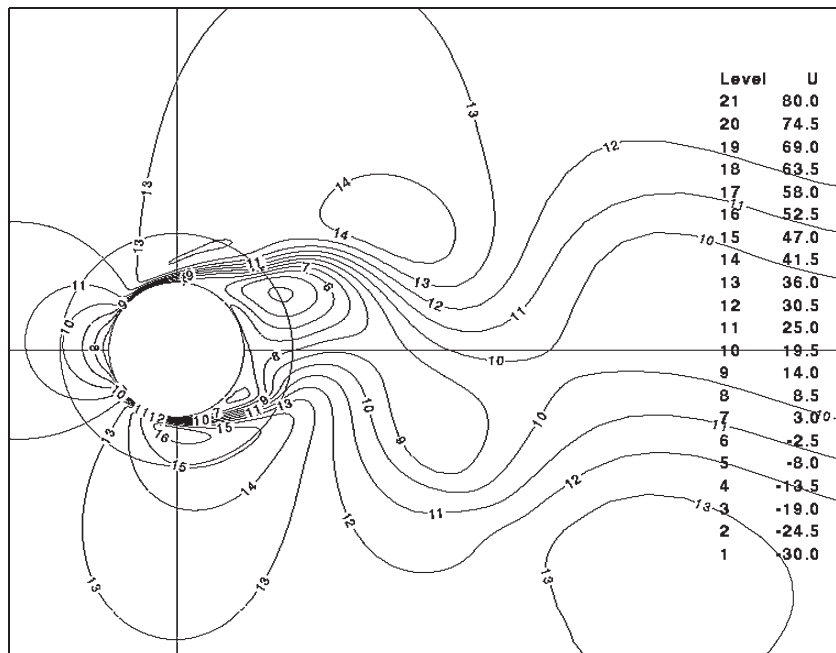
Figure 3. Velocity distribution in streamwise direction computed with the unsteady two-dimensional procedure

The predicted values for the Strouhal number in this case are presented in Table 1.

Table 1. Experimental and numerical drag coefficients and Strouhal numbers for the flow past a circular cylinder

Transition fixed at $\alpha = 80°$ for all calculations	c_D	St_{cl}
Experiment Lienhard	$0.77 - 1.4$	$0.16 - 0.225$
Experiment Cantwell and Coles	1.237	0.179
Launder and Sharma Model (linear)	0.95	0.226
Craft *et al.* Model (non-linear)	0.91	0.215

Both turbulence models overpredict the Strouhal number $St_{cl} = 0.179$ found experimentally by Cantwell and Coles but they are within the range measured by Lienhard ($St_{cl} = 0.16 - 0.225$). They also underpredict the drag coefficient measured by Cantwell and Coles ($c_D = 1.237$). A strong dependence of the drag from the transition point has been

found by imposing the transition point more downstream ($\alpha = 90°$). This gave drag coefficients values higher than the measured one – $c_D = 1.55$ for the linear model and $c_D = 1.65$ for the non-linear model. The surface pressure distribution is compared with the experimental measurements in Figure 4.
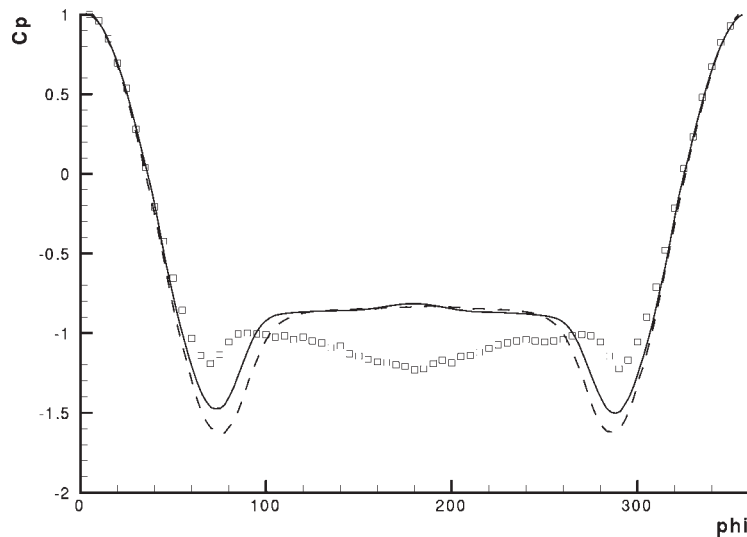

Figure 4. Mean pressure distribution on the circular cylinder calculated with Launder and Sharma model (dashed line) and Craft, Launder and Suga model (solid line); squares – experiment

Both URANS simulations predict an overshoot in the $\alpha = 90°$ region followed by a higher pressure recovery in the wake of the cylinder $90° < \alpha < 270°$ compared to the experiment. The large dependency of the turbulent length scale specified in the freestream and the resulting transition region has been confirmed by calculations with different turbulence length scales showing mean total drag variations of more than 50% in both directions and even suppression of the vortex shedding.

In addition there are strong three-dimensional vortices in the wake of the cylinder [32] which can not be resolved by a two-dimensional simulation, and this contributes also to the poor agreement. The LES with the adaptive model conducted on the coarse grid (27 000 points) showed also no vortex shedding. The maximum value of the ratio between the eddy viscosity and the molecular viscosity was approximately $v_t = 130$. The vortex generation process starts to develop only in the semi-refined grid (about 210 000 points) at a maximum value of the eddy viscosity ratio in the order of $v_t = 50$. On the finest grid the maximum eddy viscosity ratio dropped below $v_t = 20$. The excessive damping of the flow instabilities was reduced and a fully three-dimensional flow field established.

This flow field is visualised in Figure 5 by showing the crossflow component in the wake (the blue isosurfaces correspond to $w = 30$ m/s while the red isosurfaces to $w = -30$ m/s).

Correspondingly the agreement of the mean pressure distribution with the experimental results shown in Figure 6 is greatly improved.

The second flow field is one of more practical relevance for turbomachines: the flow past the VKI-turbine blade with a thick trailing edge [33]. The measurements are due to
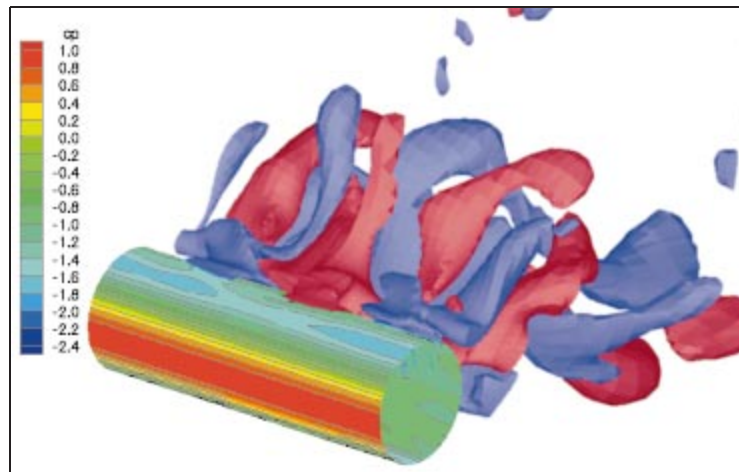
Figure 5. Crossflow velocity isosurface in the wake of the circular cylinder
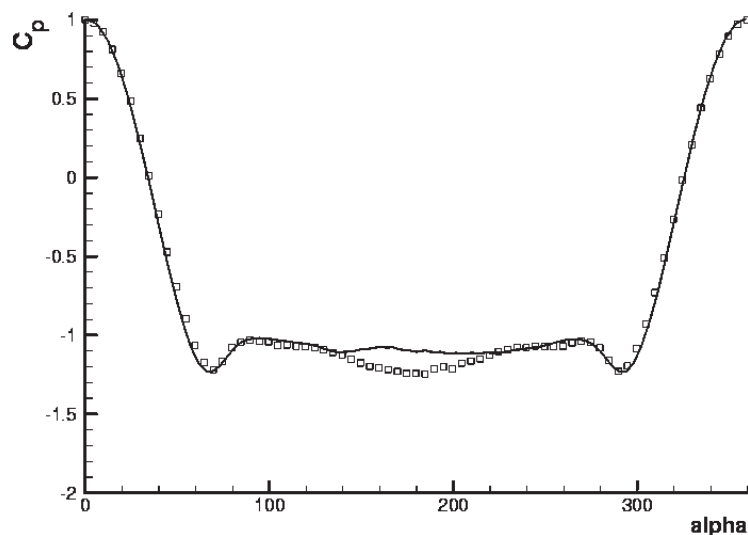calculated with the adaptive model

Figure 6. Mean pressure distribution on circular cylinder calculated
with the adaptive model (solid line); squares – experiment

Ubaldi *et al.* [34]. The Reynolds numbers were computed on the basis of chord length
$s = 0.3$ m and isentropic exit Mach number.

Four RANS simulations have been conducted: two in the subsonic range at an
isentropic exit Mach number of $\mathrm{Ma}_{2is} = 0.23$ – one using the linear model and another
using the non-linear model – and in the same way another two for the transonic range
$\mathrm{Ma}_{2is} = 0.79$. Calculations with the adaptive model were performed only in the subsonic
case. The finest grid generated for this case has 72 000 points. Only one blade has been
calculated using periodic boundary conditions.

In the subsonic flow at $\mathrm{Re} = 1.6 \times 10^6$, the measured turbulence level was $Tu = 3\%$.
The turbulence length scale has not been measured. Instead, in contrast to the cylinder flow
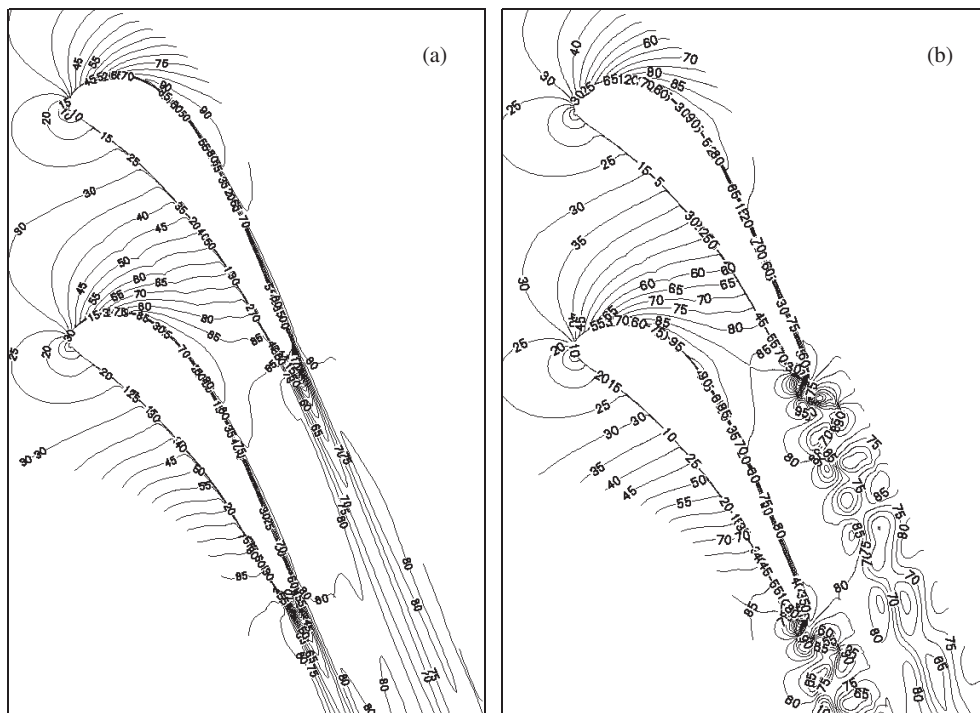
Figure 7. Contours of velocity magnitude of VKI turbine blade, units in m/s;
(a) Launder and Sharma model; (b) Craft *et al.* model

the decay of the turbulent kinetic energy along the turbine blade has been measured and a turbulence length scale of $L_t = 0.018$ m was applied at the upstream boundary in order to match these values.

A mesh convergence study has been made with a total of four different grids (1 100, 4 500, 18 000 and 72 000 points). The solution on the grid with 18 000 points and 72 000 points showed almost the same results proving the grid independence of the solution.

The experiments indicated that the wake has a periodic nature with a frequency of about 1700 Hz for the flow field with natural transition. The calculation with the linear Launder and Sharma model predicted a steady flow field (Figure 7a). The reason was the high level of eddy viscosity (Figure 8a) which suppressed all flow instabilities. The hypothesis of excessive damping due to eddy viscosity was revealed by conducting calculations without a turbulence model. This laminar calculation showed a vortex shedding frequency of about 1652 Hz.

With the non-linear as well as the adaptive model the vortex shedding process appeared on the coarse grid (4 500 point) but with a very small extention in the near wake of the trailing edge. At the semi-refined mesh (18 000 points) the vortex region extended considerably and remained almost equal on the finest grid.

The influence of two integration schemes, a 2nd and a 4th order cell centered scheme has been investigated next. The comparative results are shown in the charts of Figure 9.

The results of the adaptive model are closest to the experiment – 1650 Hz for the 4th order scheme and 1560 Hz for the 2nd order scheme. The non-linear model of Craft,
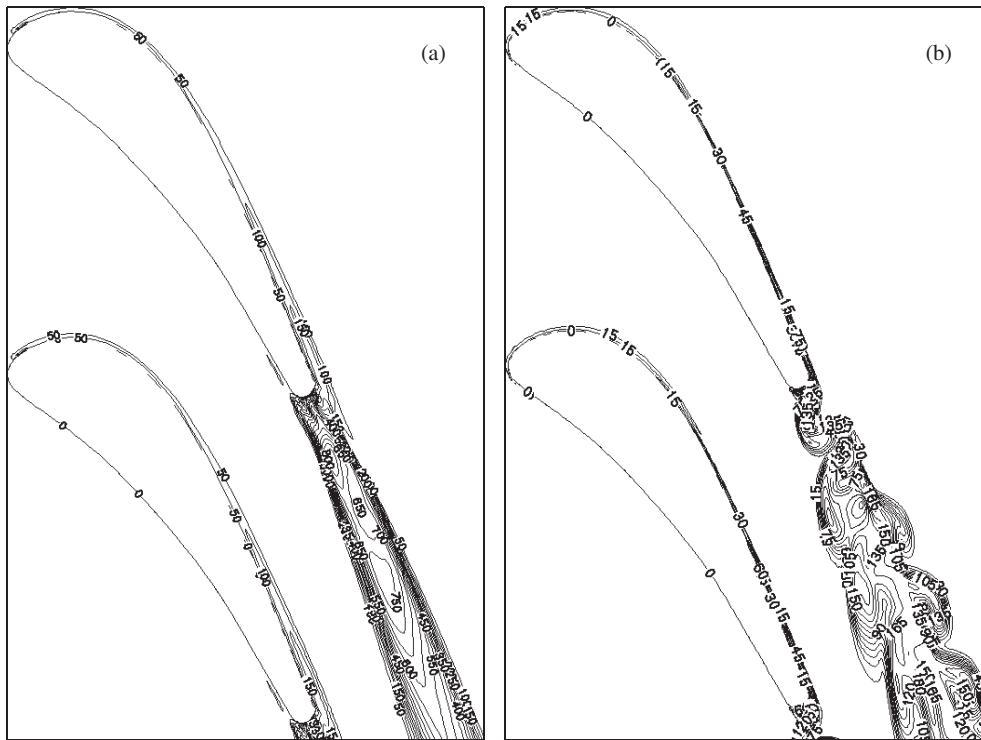
Figure 8. Contours of eddy viscosity ratio of VKI turbine blade, units in m/s;
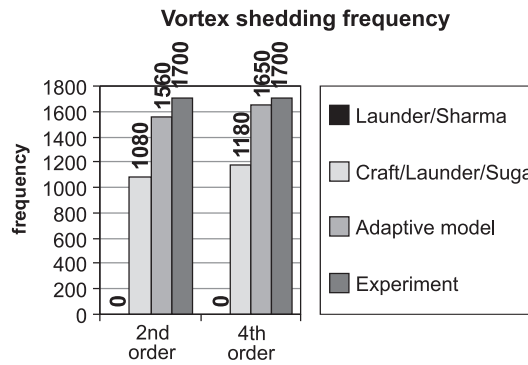(a) Launder and Sharma model; (b) Craft *et al.* model

Figure 9. Vortex shedding frequency determined experimentally and numerically

Launder and Suga gave 1180 Hz and 1080 Hz, respectively, while the linear model failed to predict vortex shedding.

The pressure distribution is not so sensitive in this case so that the results obtained with the different models are all in good agreement with the experiment and close to each other.

The velocity profile of the linear equation disagrees with the experimental profiles due to the high eddy viscosity and hence the turbulence stress in the boundary layer (Figure 10a). The velocity profiles obtained with the non-linear as well as with the adaptive model are in much better agreement with the experimental ones (Figure 10b).

For the transonic flow the same grid as for the subsonic flow was used but scaled to a chord length of $c = 0.140$ m. The upstream total pressure was $p_t = 1.4$ bar and the total temperature was $T_t = 280$ K. The turbulent kinetic energy was 1.2%. Because the turbulent length scale was not measured it was chosen like in the case of cylinder such that the eddy viscosity was of the order of the laminar viscosity.

The first calculation was done on the coarse grid with 5 000 points. In order to speed up the calculation in the transient phase, the first few hundred iterations were performed with a high time step $\Delta t = 1$ ms. In order to capture the frequency of about $F = 7500$ Hz the time step has been subsequently reduced to $\Delta t = 0.03$ ms. Again due to numerical dissipation and truncation errors in the coarse grid the predicted flow field was steady. The vortex shedding process started only on the second finest grid (18 000). The computed Strouhal number and the frequency was close to that determined experimentally: St = 0.229 and $F = 7710$ Hz, respectively, in comparison to St = 0.225 and $F = 7500$ Hz. The finest mesh (72 000 points) gave even better results St = 0.224 and $F = 7450$ Hz.
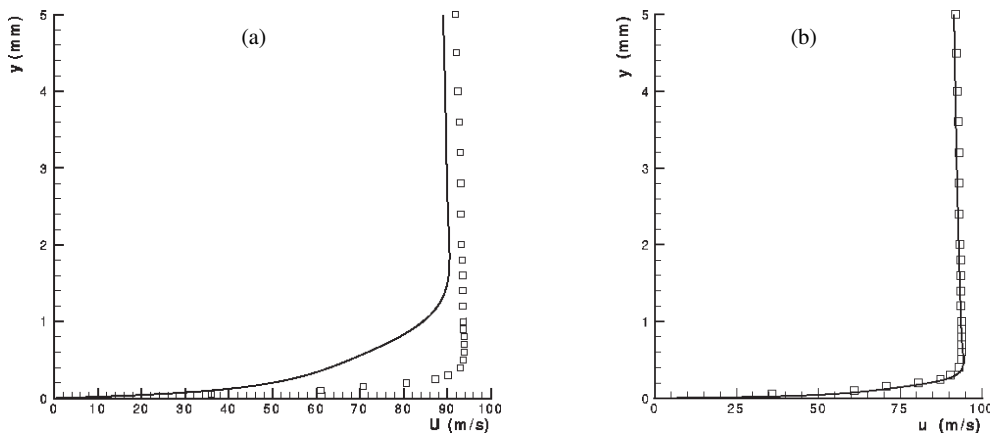

Figure 10. Mean velocity profile calculated at 30% chord with:
(a) linear two equation model; (b) adaptive two equation model

Figure 11 compares the Mach number distribution from the simulation with the measurements. On the suction side and in the rear pressure side of the blade the numerical results are very close to the experiment. Contrary to very good results generally obtained by CFD codes for favorable pressure gradient flows, the simulation predicts lower values in the front part of the pressure side.

Qualitatively both the measurement and the calculation show a peculiar pressure jump at upper and lower junction between the trailing edge and the rear part of the blade as shown in Figure 12.

One possible physical effect that can be responsible for this is a shock wave forming at the trailing which interacts with the vortex shedding process.

This explanation can be supported by performing a steady state calculation that should not show this jump. Differences between the two calculations are only around the trailing edge (see Figure 13).

A possible explanation is that the vortex shedding from the trailing edge in the unsteady simulation induces a flow which must accelerate around the trailing edge much
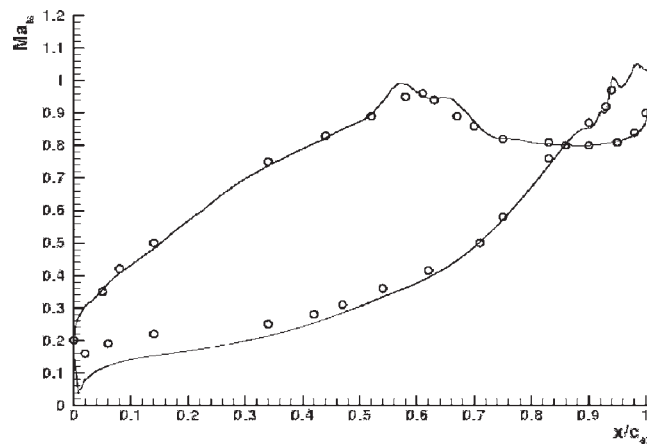
Figure 11. Comparison between unsteady calculation and experimental Mach numbers for the VKI profile in transonic flow
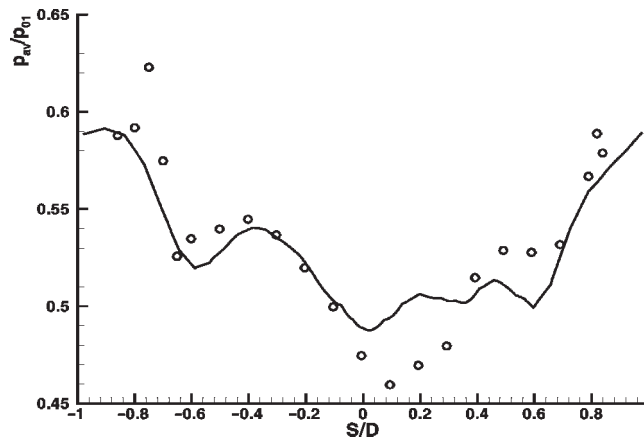

Figure 12. Comparison between unsteady calculation and experimental pressure ratio for the VKI profile in transonic flow
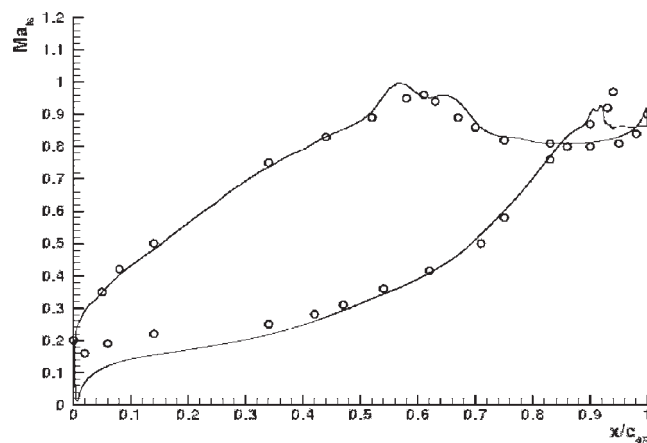

Figure 13. Comparison between steady calculation and experimental Mach numbers for the VKI profile in transonic flow
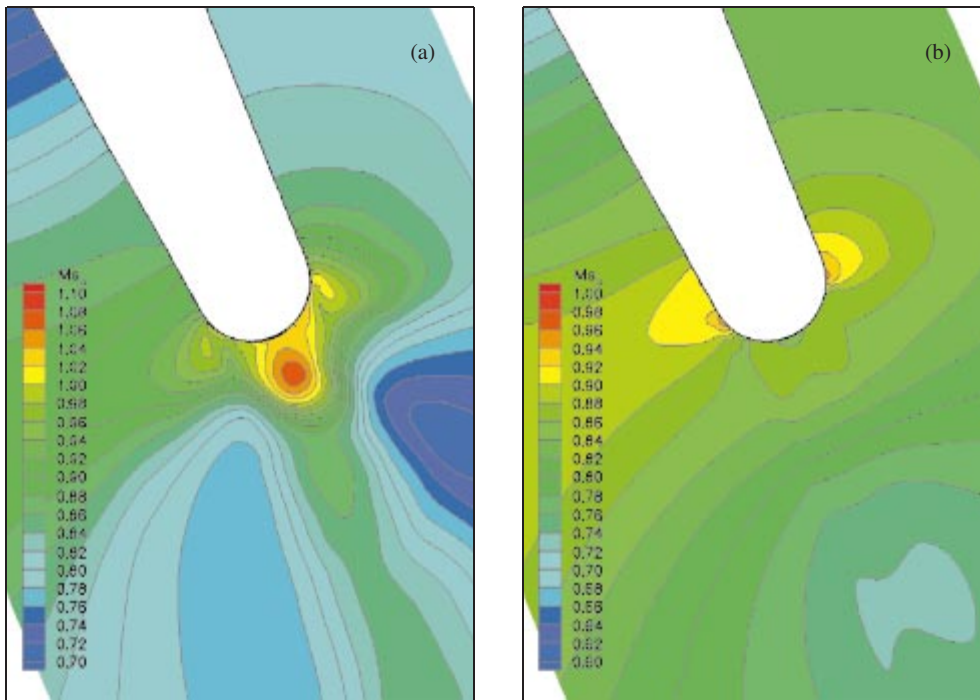
Figure 14. Mean isentropic Mach number contours for the transonic flow past the VKI profile:
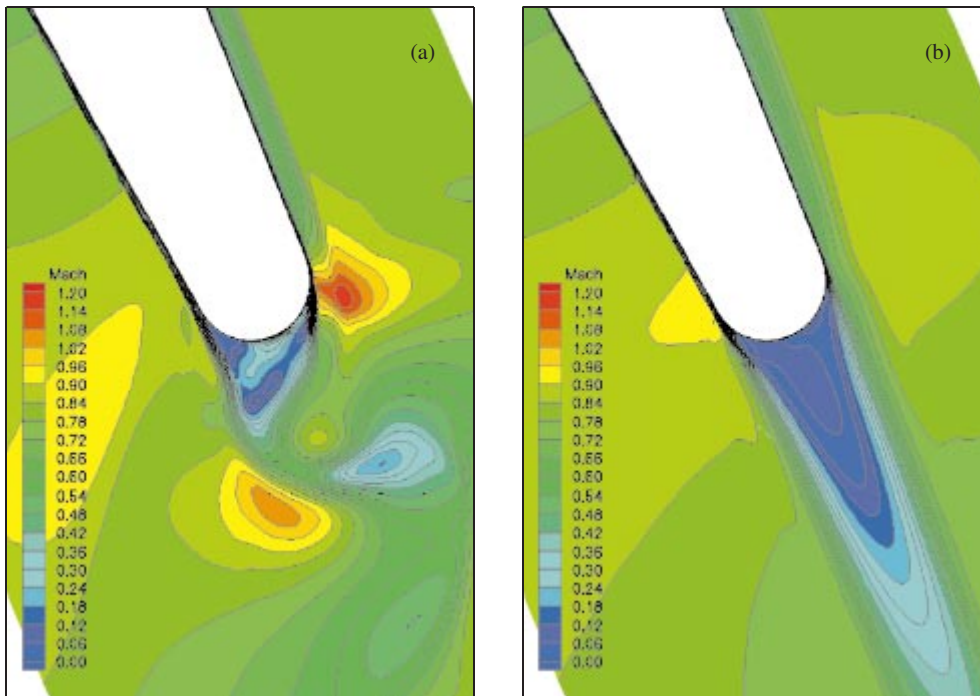(a) unsteady calculation; (b) steady calculation

Figure 15. Mach number contours for the transonic flow past the VKI profile:
(a) instantaneous Mach number contours; (b) steady Mach number contours

higher than in the steady state calculation in order to refill the wake (where a lower pressure is induced like the isentropic Mach number contours shown in Figure 14). That is marked out by the Mach number distribution which is convex in the unsteady simulation and concave in the steady state simulation.

In the unsteady calculation the flow becomes locally supersonic (Ma = 1.15) while in the steady state it remains subsonic everywhere. The connection between this phenomenon and the pressure jump must be further investigated in more details.

5. Conclusions

The paper presented a number of turbulence models which try to increase the prediction capability of CFD methods. Combining unsteady calculations with an appropriate turbulence model it can capture the particularities much better than steady state calculations. Since the flow over a cylinder is highly three-dimensional in the near wake, it is obvious that a two-dimensional calculation is inappropriate for this flow. This type of calculation can not reproduce the pairs of counter-rotating streamwise vortices observed in the experiment and therefore is inaccurate.

The flow past the VKI blade is only modestly three dimensional but in this case the non-linearity of the turbulence model is required because large anisotropic stresses dominate the turbulence field. It has been shown that two-dimensional unsteady calculations match the experimental results better than steady state calculations.

A recently proposed adaptive model gave very good results for the cylinder as well as the subsonic turbine calculation. The novelties of this model are:

- if all turbulent fluctuations are resolved it gives the correct asymptotically limit of a DNS and if no fluctuations at all are resolved it reduces to a statistical turbulence model,
- the flexibility – any two equation turbulence model that solves transport equations for the turbulent kinetic energy k and either the dissipation rate ε, the turbulent time scale τ or the inverse time scale ω can be used as a basis for it,
- the inclusion of a stochastic backscatter model that models the energy transfer from the small scales to the large scales.

References

[1] Chen W L and Leschziner M 1999 *Turbulence modelling of rotor/stator interaction with linear and non-linear eddy-viscosity models* Third European Conference on Turbomachinery: Fluid Dynamics and Thermodynamics **A**, pp. 259–268

[2] Magagnato F 1999 *Unsteady Flow Past a Turbine Blade Using Non-linear Two-equation Turbulence Models* Third European Conference on Turbomachinery: Fluid Dynamics and Thermodynamics **A**, pp. 221–230

[3] Magagnato F and Gabi M 2000 *A new adaptive turbulence model for unsteady flow fields in rotating machinery* Proceedings of ISROMAC-8 **1** 413

[4] Piomelli U 1997 *Introduction to the modelling of turbulence* von Karman Institute for Fluid Dynamics, Lecture Series

[5] Smagorinsky J 1963 *Mon. Weather Review* **91** 91

[6] Baldwin B S and Lomax H 1978 *Thin Layer Approximation and Algebraic Model for Separated Turbulent Flows* AIAA Paper 78–257

[7] Germano M 1992 *J. Fluid Mech.* **238** 325

[8] Launder B and Sharma B I 1974 *Letters in Heat and Mass Transfer* **1** (2) 131

[9] Speziale C G, Abid R and Anderson E C 1990 *A Critical Evaluation of Two-Equation Models for Near Wall Turbulence* ICASE Report No. 90–46

[10] Speziale C G 1987 *Journal of Fluid Mechanics* **178** 458

[11] Magagnato F 1995 *Untersuchung von linearen und nichtlinearen Wirbelviskositätsmodellen* Dissertation TH-Darmstadt

[12] Launder B E 1996 *Turbulence and Transition Modelling* Kluwer Academic Publishers

[13] Craft T J, Launder B E and Suga K 1995 *A Non-linear Eddy Viscosity Model including Sensitivity to Stress Anisotropy* 10th Symposium Turbulent Shear Flows, Pennsylvania State University

[14] Bourkovskaia L 1997 *Anwendung nichtreflektierender Randbedingungen zur Berechnung kompressibler Strömungen nach der Finiten Volumen Methode* Diplomarbeit Uni-Karlsruhe

[15] Rudy D H and Strikwerda J C 1980 *J. Comput. Phys.* **36** 55

[16] Poinsot T J and Lele S K 1992 *J. Comput. Phys.* **101** 104

[17] Zunino P 1996 *Time varying wake flow characteristics behind flat plates and turbine cascades* Final report, Brite EURAM AER2-92-0048

[18] Speziale C G 1998 *AIAA Journal* **36** (2) 173

[19] Spalart P R, Jou W-H, Strelets M and Allmaras S R 1997 *Comments on the Feasibility of LES for Wings, and on a Hybrid RANS/LES Approach* First AFORS Intern. Conference on Direct Numerical Simulation and Large Eddy Simulation

[20] Spalart P R and Allmaras S R 1994 *La Recherche Aerospatiale* **1** 5

[21] Lilly D K 1967 *The Representation of Small-scale Turbulence in Numerical Simulation Experiments* Proc. IBM Sci. Comput. Symp. On Environmental Sci., pp. 195–210

[22] Leith C E 1990 *Phys. Fluids* **A 2** 297

[23] Mason P J and Thomson D J 1992 *Journal of Fluid Mechanics* **242** 51

[24] Schumann U 1995 *Proc. R. Soc. London.* **A 451** 293

[25] Magagnato F 1998 *TASK Quarterly* **2** (2) 215

[26] Jameson A 1991 *Time Dependent Calculations Using Multigrid, with Applications to Unsteady Flows Past Airfoils and Wings* AIAA Paper 91–1596

[27] Arnone A, Liou M S and Povinelli L A 1995 *AIAA Journal* **33** (6) 985

[28] Jameson A, Schmidt W and Turkel E 1981 *Numerical Solution of the Euler Equations by Finite Volume Methods using Runge-Kutta Time-Stepping Schemes* AIAA Paper 81–1259

[29] Jameson A 1985 *Multigrid Algorithms for Compressible Flow Calculations* Technical Report 1743, MAE-Report

[30] Lienhard J H 1966 *Synopsis of Lift, Drag and Vortex Frequency for Rigid Circular Cylinders* College of Engineering Research Division Bulletin 300, Tech. Extension Service, Washington State University

[31] Cantwell B and Coles D 1983 *Journal of Fluid Mechanics* **136** 321

[32] Beaudan P and Moin P 1994 *Numerical Experiments on the Flow Past Circular Cylinder at Sub-critical Reynolds Number* Report No. TF-62, Stanford University, California

[33] Cicatelli G and Sieverding C H 1996 *The Effects of Vortex Shedding on the Unsteady Pressure Distribution around the Trailing Edge of a Turbine Cascade* ASME Paper no. 96-GT-359

[34] Ubaldi M, Zunino P, Campora U and Chiglione A 1996 *Detailed Velocity and Turbulence Measurements of the Profile Boundary Layers in a Large Scale Turbine Cascade* ASME Journal 96-GT-42